

# Single-atom catalysts boost nitrogen electroreduction reaction

Yanling Zhai<sup>a,b,†</sup>, Zhijun Zhu<sup>\*a,†</sup>, Chengzhou Zhu<sup>c</sup>, Xueji Zhang<sup>\*b,d</sup>, Jing Tang<sup>\*e</sup>, and Jun Chen<sup>\*f</sup>

<sup>a</sup>College of Chemistry and Chemical Engineering, Institute of Hybrid Materials, College of Materials Science and Engineering, Qingdao University, Qingdao 266071, P.R. China.

<sup>b</sup>Research Center for Intelligent and Wearable Technology, Qingdao University, Qingdao 266071, P.R. China.

<sup>c</sup>College of Chemistry, Central China Normal University, Wuhan 430079, P.R. China

<sup>d</sup>School of Biomedical Engineering, Shenzhen University Health Science Center, Shenzhen, Guangdong 518060, P.R. China.

<sup>e</sup>Department of Materials Science and Engineering, Stanford University, Stanford, CA 94305, USA.

<sup>f</sup>Department of Bioengineering, University of California, Los Angeles, CA 90095, USA.

<sup>†</sup>These authors contributed equally to this work.

\*Correspondence and requests for materials should be addressed to J.T. (jingtang@stanford.edu) or X.Z. (zhangxueji@szu.edu.cn) or Z.Z. (zhuzhijun@qdu.edu.cn) or J.C. (jun.chen@ucla.edu)

## Abstract

Ammonia ( $\text{NH}_3$ ) is mainly produced through the traditional Haber-Bosch process under the harsh conditions with huge energy consumption and massive carbon dioxide ( $\text{CO}_2$ ) emission. The nitrogen electroreduction reaction (NERR), as an energy-efficient and environment-friendly process converting nitrogen ( $\text{N}_2$ ) to  $\text{NH}_3$  under ambient conditions, has been regarded as a promising alternative to the Haber-Bosch process and has received enormous interest in recent years. Although some exciting progress has been made, considerable scientific and technical challenges still exist in improving the  $\text{NH}_3$  yield rate and Faradic efficiency, understanding the mechanism and promoting the wide commercialization of NERR. Single-atom catalysts (SACs) have emerged as promising catalysts because of the atomically dispersed activity sites and maximized atom efficiency, unsaturated coordination environment, and the unique electronic structure, which could significantly improve the rate of reaction and yield rate of  $\text{NH}_3$ . In this review we briefly introduce the unique structural and electronic features of SACs, which help to comprehensively understand the mechanism due to their structural simplicity and diversity, and in turn expedites the rational design of fantastic catalysts at the atomic scale. Then we mainly summarize the most recent experimental and computational efforts on developing novel SACs with excellent NERR performance, including precious metal-, nonprecious metal- and nonmetal-based SACs. Finally, the challenges and perspectives of SACs on NERR, as well as some potential means for advanced NERR catalysts are present.

## 1. Introduction

As one of the most important raw material used in agriculture and chemical industry, ammonia ( $\text{NH}_3$ ) is mainly synthesized from pure hydrogen gas ( $\text{H}_2$ ) and nitrogen ( $\text{N}_2$ ) through a traditional Haber-Bosch process conducted under extremely harsh conditions ( $\sim 40$  MPa,  $\sim 500$  °C), which consumes nearly 2% of global energy supply.<sup>1</sup> In traditional  $\text{NH}_3$  production, about 75% of energy input is used for  $\text{H}_2$  generation from steam reforming, and residual energy is applied to Haber-Bosch process, including gas compression,  $\text{NH}_3$  synthesis and post-separation, accompanied by the emission of 1% global greenhouse gas, carbon dioxide ( $\text{CO}_2$ ) (Fig. 1A). In view of the fossil fuel scarcity and global climate change, an energy-efficient and environment-friendly process for converting  $\text{N}_2$  into  $\text{NH}_3$  under ambient conditions is highly desirable. As an alternative approach to Haber-Bosch process, electrocatalytic synthesis of  $\text{NH}_3$  directly from  $\text{N}_2$  and  $\text{H}_2\text{O}$  has attracted considerable attention because the electrochemical process can be conducted under ambient conditions (without  $\text{H}_2$  supply) and powered by renewable energy sources (Fig. 1B).<sup>2</sup> Benefiting from the advantages of  $\text{N}_2$  electroreduction reaction (NERR) such as a mild reaction condition, high energy efficiency, without  $\text{CO}_2$  emission and fossil fuel consumption and so on, exploring smart design to synthesize efficient catalysts toward NERR has attracted growing interest.<sup>3</sup>

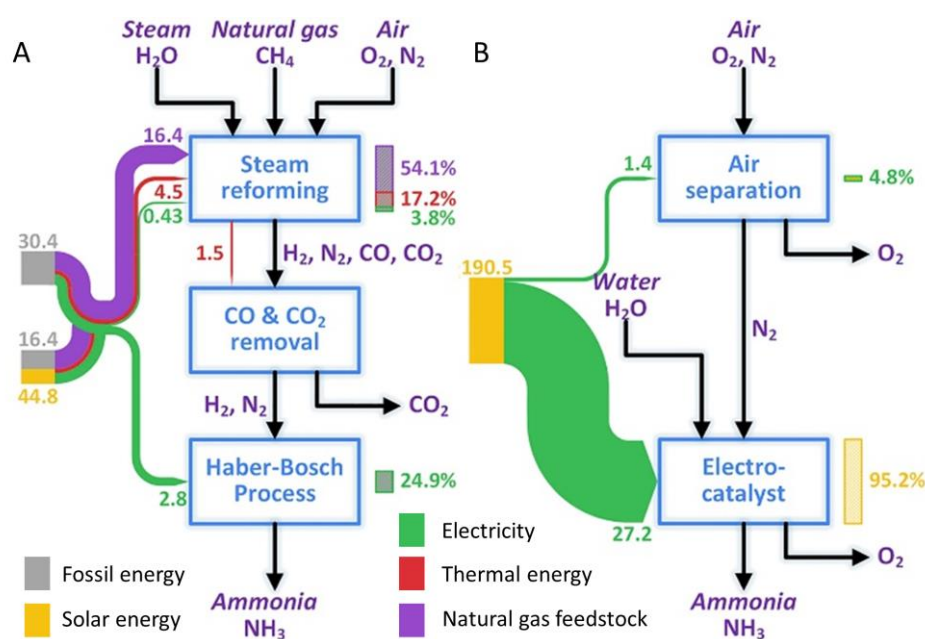


**Fig. 1** The energy-efficiency analysis for different approaches. (A) Conventional Haber-Bosch approach and electrochemical approach (B). Reproduced with permission from ref. <sup>4</sup>. Copyright 2018, Elsevier Ltd.

The overall NERR reaction can be depicted as:  $\text{N}_2 + 3\text{H}_2\text{O} \rightarrow 2\text{NH}_3 + 3/2 \text{O}_2$ ,<sup>5</sup> during which  $\text{N}_2$  reacts with  $\text{H}_2\text{O}$  to produce  $\text{NH}_3$  and  $\text{O}_2$ . NERR has a similar theoretical potential to that of hydrogen evolution reaction (HER),<sup>6</sup> which creates a fundamental problem for electrochemical ammonia synthesis. NERR is typically plagued by the low affinity of  $\text{N}_2$  on the catalysts, the fast reaction kinetics of competing HER,<sup>7</sup> much higher concentration of H than

that of  $N_2$  in aqueous solution and high bond energy of  $N\equiv N$  (941 kJ/mol), which always leads to a low  $NH_3$  yield rate and a poor Faradaic efficiency (FE).<sup>8, 9</sup> Particularly, HER always becomes the dominant process under highly negative potentials. Therefore, increasing efforts have been devoted to exploring catalysts with efficient NERR performance to improve the selectivity and reaction rate.

The size of nanostructures shows a significant influence on their NERR performance. As reported by Shi and coworkers, Au nanoclusters with a diameter of 0.5 nm supported on  $TiO_2$  exhibited the better NERR performance than other sizes (37 and 4 nm) regarding  $NH_3$  yield rate, FE and selectivity, which was ascribed to the subnanometer size and the high dispersion of the Au nanocluster.<sup>10</sup> It is reasonable to expect that continuously minimizing the size of monodispersed Au nanocluster on the substrate will lead to much improved catalytic performance because the atomically dispersed catalysts show the maximized interface of every single atom.<sup>11</sup> Besides, decreasing the size of catalysts will lead to an increased fraction of exposed atoms with unsaturated coordination sites, which have been proved to enhance the activity of electrocatalysts. Therefore, single atoms stabilized by supports would be promising candidates for NERR catalysts because of their maximized atom efficiency, unsaturated metal coordination environment, and unique electronic structures.<sup>7</sup>

Great efforts have been devoted to exploring single-atom catalysts (SACs) for NERR. 1) SACs possess a similar structure to molecular catalysts showing high activity toward  $N_2$  reduction, in which metal centers are coordinated by ligands. 2) Numerous couples of different atomic centers and various substrates would extend the sample capacity for mechanism investigation of NERR.<sup>12</sup> Although some excellent review articles have been published in terms of the synthesis of the novel catalysts and their applications in NERR,<sup>13, 14</sup> few of them have paid special attention to the SACs.<sup>15</sup> Inspired by great advantages of SACs and accumulated publications on SACs with high NERR performance, we summarize the most recent experimental and theoretical development of SACs for NERR under ambient conditions during the past few years. Firstly, the unique structural and electronic features of SACs are briefly introduced. Furthermore, we focus on the most recent advances in the development of NERR SACs classified by the type of active centers. Finally, the major challenges and perspectives for future research on the design of efficient SACs for NERR and optimization of their electrocatalytic performance are present. We expect that this review could inspire further interest in investigating the synthesis of novel NERR SACs, thereby offering opportunities in this emerging research area.

## 2. Single-atom catalysts

SACs are a kind of emerging catalysts, which are composed of isolated single atoms (both metallic and nonmetallic ones) stabilized on the supports. SACs have attracted increasing attention over the past several years since they were first proposed by Zhang and coworkers,<sup>16</sup> because they exhibit superior catalytic performance to their conventional counterparts in a range of reactions. SACs are synthesized through various wet-chemistry approaches, including

spatial confinement, defect engineering, and coordination design strategies.<sup>17</sup> The single atoms are usually trapped by the defects or vacancies of the supports. The support offers a unique local environment of the single atoms through the strong interaction between single atom and support, such as unsaturated coordination and unique electronic structure,<sup>16</sup> which leads to large exposed active sites, maximized atom-utilization efficiency and thus enhanced intrinsic catalytic activity and the low cost of the electrocatalysts.<sup>18</sup> With an aid of theoretical calculation, SACs are employed to reveal the mechanism of a given reaction because of structural simplicity and homogeneity of a given SAC, which in turn promotes a comprehensive understanding of the synergetic effect of single atoms and supports and expedites the rational design of fantastic catalysts at the atomic scale. Recently, SACs have emerged as very promising catalysts for a range of reactions, such as oxygen reduction reaction,<sup>19</sup> HER,<sup>20</sup> oxygen evolution reaction,<sup>21</sup> CO oxidation reaction,<sup>16</sup> CO<sub>2</sub> reduction reaction,<sup>22</sup> and so on.<sup>18</sup> Most recently, taking advantage of the outstanding features of SACs and the unsatisfying performance of regular catalysts in NERR, researchers have turned their attention to the SAC-based NERR catalysis.

### 3. Pre-screening of NERR SACs based on calculation

Developing efficient, economical, and durable electrocatalysts is essential and significant for the rapid development and commercial application of NERR technology. Interactions between single atoms and supports are critical to the electrocatalytic activity and stability of the SACs because there is a trade-off between diffusion and aggregation of single atoms, especially the metal ones.<sup>23</sup> N-containing substrates, such as C<sub>3</sub>N<sub>4</sub>, N-doped graphene (NG), N-doped carbon (NC), N-doped porous carbon (NPC), zeolitic imidazolate frameworks (ZIF) and metal oxide with defects have been explored to stabilize single metal atoms because of their open porous structure, large surface area, abundant N species, plentiful metal and oxygen vacancies, which could provide large possibilities to anchor and stabilize the single atoms and the mass transport during the electrochemical reaction.<sup>24</sup> In spite of the progress has been made, it remains a great challenge to synthesize the ideal SACs for NERR due to the lack of appropriate synthesis method. Alternately, density functional theory (DFT) calculation contributes to evaluate the activity of single atoms stabilized by the supports with a well-defined structure. To screen the NERR catalysts among the NG supported single metal atoms (**Fig. 2A-E**) more efficiently, Wang and coworkers proposed a general two-step strategy-based calculation (**Fig. 2A**) instead of determining all the reaction intermediates. The two-steps strategy involves (1) N<sub>2</sub> capture and hydrogenation to N<sub>2</sub>H, and (2) NH<sub>3</sub> generation from NH<sub>2</sub> and subsequent desorption. Considering the two types of N<sub>2</sub> adsorption configurations (side-on and end-on), nine potential metal-NG coordination possibilities (**Fig. 2B**), and 30 kinds of metals (**Fig. 2C**), there are 540 possibilities. The N<sub>2</sub> adsorption energies ( $\Delta E_{N_2}$ ) on different catalysts are shown in **Fig. 2D**. The  $\Delta E_{N_2}$  is highly related to the group number, the number of unoccupied d orbitals and the d electrons of metals, as well as the coordination structures between metals and graphene substrates. After the energies calculation by evaluating the two key factors in each step, 10 promising candidates (**Fig. 2E**) with excellent NERR performances were selected. Among them, single W atoms with three C coordination (W<sub>1</sub>C<sub>3</sub>) afforded the best NERR activity. In addition

to providing a series of promising SACs for NERR, this work proposed a simplified approach for screening the catalysts toward NERR.

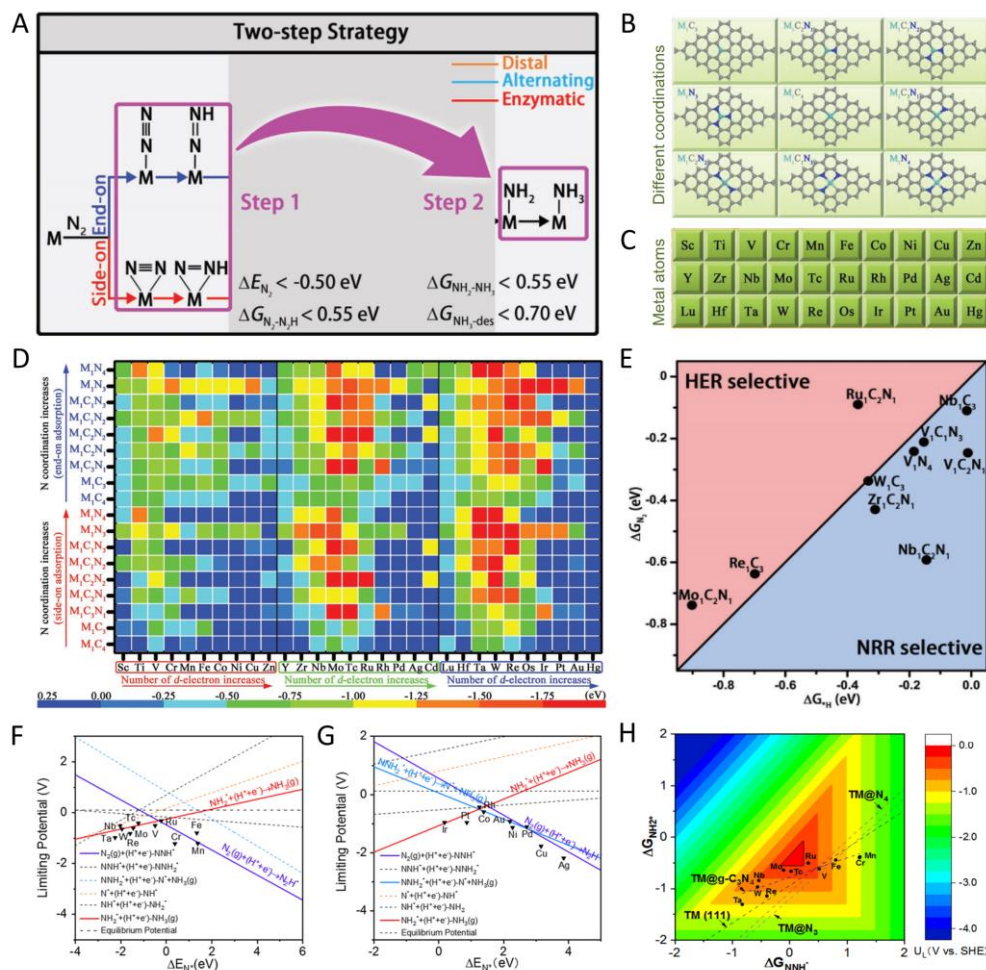


**Fig. 2** Calculation-based screening of NERR SACs. (A) Diagram of the two-step screening method. Proposed structures of NG-supported SACs with different coordination (B) and 30 kinds of transition metals (C). (D) Adsorption energies of N<sub>2</sub> on different SACs through side-on and end-on configurations. (E) Calculated adsorption free energies of H and N<sub>2</sub> on the selected SACs. Reproduced with permission from ref. <sup>25</sup>. Copyright 2018, Elsevier Ltd. (F-G) The relationship between limiting potential and the adsorption energy of \*N ( $\Delta E_{N^*}$ ) at 0 V for early (F) and late (G) TMs. \* represents an adsorption state. (H) Color-filled contour plots of the limiting potential as a function of the Gibbs free energy of the key intermediates (\*NNH and \*NH<sub>2</sub>) on the SACs with different compositions (metal centers and supports). Reproduced with permission from ref. <sup>12</sup>. Copyright 2019, American Chemical Society.

Most reported NERR catalysts suffer from low activity and poor FE, which greatly limited the development of NERR. A deep understanding of the mechanism could guide the rational design of the NERR catalysts. Most recently, Qiao and coworkers have carried out DFT simulations to build a profile of the potential SACs for NERR in consideration of the activity trends, electronic origins, and design strategies of the SACs.<sup>12</sup> The intrinsic activity of SACs was found to be highly related to the adsorption energy of N ( $\Delta E_{N^*}$ , **Fig. 2F and G**). The

variations of  $\Delta E_{N^*}$  on transition metals (TMs) originate from the bonding/antibonding orbital populations. The support shows great influence on the NERR activity by introducing various ligand effects. The influences of electronic environments of 20 TMs on the activity of SACs were evaluated by using three kinds of NC substrates, g-C<sub>3</sub>N<sub>4</sub>, and carbon with different coordinating N atoms in NC. The limiting potential of SACs highly depends on the adsorption strength of key intermediates (**Fig. 2H**), because of the variation of the electronic structure of the SACs. Consequently, the suitable match between metal center and support, as well as the subsequent regulation of adsorption strength of the key intermediates are critical for the rational design of the NERR SACs. In addition, stability and selectivity should be taken into accounts for catalyst design. As an example, single Ru and Rh atoms supported on g-C<sub>3</sub>N<sub>4</sub> have been predicted as potential NERR catalysts over 60 candidates. This work made a contribution to the development of more efficient SACs for NERR.

## 4. Application of SACs in NERR

### 4.1 TM-based SCAs

TM-based catalysts show excellent activity to NERR because on the one hand, these TM atoms have empty *d* orbitals to accept the lone pair electrons of N<sub>2</sub>, on the other hand, TM atoms could donate *d* electrons to the antibonding orbitals of N<sub>2</sub> and weaken the N≡N bond. Therefore, TMs with both empty and occupied *d* orbitals might be promising components for efficient NERR catalysts.<sup>26</sup>

#### 4.1.1 Precious metal-based SACs

Pt has been considered as a universal effective catalyst component for many reactions, however, Pt-based catalysts do not show appreciable activity for NERR in aqueous solution. Firstly, Pt shows a much higher affinity to H than N. Secondly, the concentration of H<sub>2</sub>O is much higher than soluble N<sub>2</sub> in aqueous systems. Both of these two factors support the fact that Pt is prone to be covered with H instead of N, thus a large overpotential is requested to active N<sub>2</sub> on Pt-based catalysts.<sup>27</sup> Fortunately, Ru- and Au-based SACs have been theoretically and experimentally proven to be efficient catalysts for NERR.

##### 4.1.1.1 Au SACs

Electrocatalytic activities of metal catalysts are highly dependent on their electronic structures, therefore the state density of *d*-band metal is usually used to evaluate their electrocatalytic activities. Zhang and coworkers investigated the relationship between the coordination number and NERR activity of the Au *via* first-principle calculations.<sup>29</sup> The NERR activity of Au is highly dependent on the coordination number of Au. The reduced coordination number of Au atoms would lead to exposed surface and enhanced electrocatalytic activity. In addition, Au has been regarded to possess a low affinity to H, evidenced by the poor HER activity.<sup>10</sup> These intrinsic features endow Au a significant NERR activity. Qin and coworkers reported single Au atoms anchored on NPC (Au SA/NPC) for NERR (**Fig. 3A**).<sup>6</sup> The single Au atoms are stabilized

by abundant N and C species with strong electronegativity, resulting in charge redistribution between Au atoms and substrate. Therefore,  $N_2$  can be bridged between positively polarized Au atoms and negatively polarized N or C atoms, which facilitates the subsequent activation of  $N_2$  by electronic polarization and further breakage of  $N\equiv N$  bond. Consequently, the as-synthesized Au SA/NPC exhibited superior activity to NERR against HER, evidenced by the large current density difference over a wide potential range (**Fig. 3B**). To better understand the specific advantages of single Au sites, AuNPs anchored on NPC (AuNP-NPC) were used as a control. At a potential of -0.2 V (vs. RHE), Au SA/NPC revealed a much higher FE of 12.3% than that of AuNP-NPC (5.7%, **Fig. 3C**). Moreover, AuNPs anchored on N-free C (AuNP/C) exhibited a decreased FE of 4.5% at the same condition (**Fig. 3C**). These results indicated that both NPC substrate and single Au atoms play crucial roles in excellent NERR performance.<sup>6</sup>

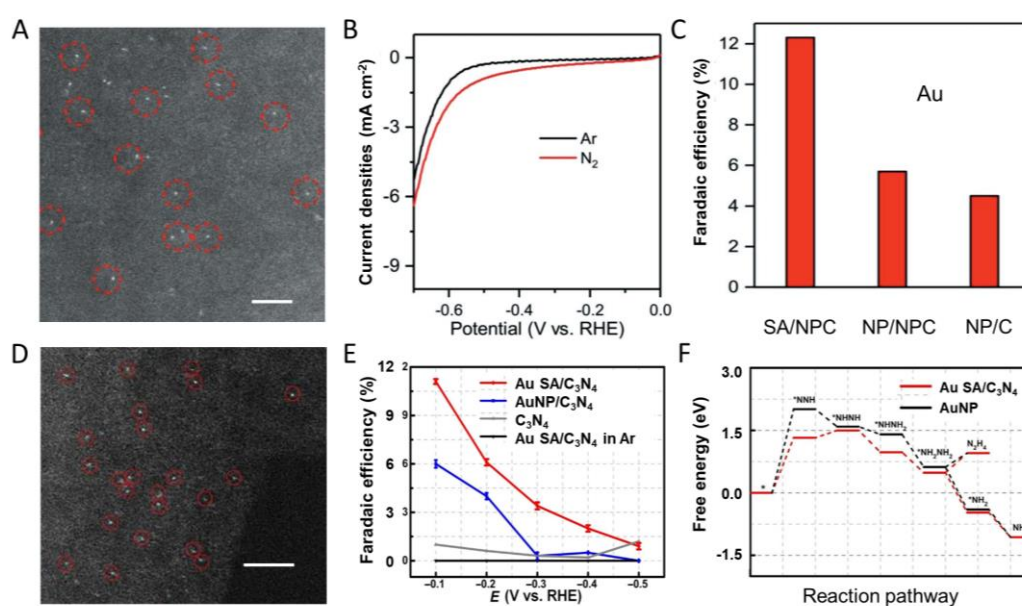


**Fig. 3** TEM images and electrocatalytic performance of the Au SACs. (A) High-magnification HAADF-STEM image of Au SA/NPC. (B) LSV curves of Au SA/NPC in 0.1 M HCl aqueous solution saturated with  $N_2$  and Ar. (C) FE values of  $NH_3$  with different catalysts at -0.2 V (vs. RHE). Reproduced with permission from ref. <sup>6</sup>. Copyright 2018, Wiley-VCH. (D) The aberration-corrected HAADF-STEM image of Au SA/ $C_3N_4$  directly shows the atomic dispersion of Au atoms, scale bar: 2 nm. (E) FE values of  $NH_4^+$  on different catalysts including Au SA/ $C_3N_4$ , AuNP/ $C_3N_4$ , pure  $C_3N_4$ , and Au SA/ $C_3N_4$  in Ar. (F) Free energy profile of NERR on Au SA/ $C_3N_4$  and Au NP (211) at 0 V. Reproduced with permission from ref. <sup>28</sup>. Copyright 2018, Elsevier Ltd.

Both activity and selectivity are required simultaneously for an eligible catalyst. Wang and coworkers synthesized  $C_3N_4$  supported single Au atoms (Au SA/ $C_3N_4$ ) through  $HAuCl_4$  adsorption and subsequent reduction under  $H_2$  atmosphere. Au NPs anchored on  $C_3N_4$  were synthesized for comparison. The bright dots circled in red in the aberration-corrected HAADF-STEM image (**Fig. 3D**) indicate the atomically distribution of Au. Au SA/ $C_3N_4$  reached a high  $NH_3$  FE than AuNP/ $C_3N_4$  and  $C_3N_4$  alone at a wide potential range (**Fig. 3E**). The free energy



profiles shown in **Fig. 3F** reveals that the first hydrogenation step (reduction of  $^*\text{N}_2$  to  $^*\text{NNH}$ ) is the rate-determining step in NERR. The large free energy difference between the two catalysts of the first step explains the high NERR performance of SACs. In addition, compared with the formation that of  $\text{NH}_3$ , the formation of  $\text{N}_2\text{H}_4$  is energetically unfavorable on both Au SAC and AuNP. Benefiting from the efficient atom utilization, Au SA/ $\text{C}_3\text{N}_4$  displays excellent NERR efficiency with an FE of 11.1% and an  $\text{NH}_4^+$  yield rate of 1,305  $\mu\text{g/h/mg}_{\text{Au}}$ , which was 22 times higher than that of AuNP/ $\text{C}_3\text{N}_4$ .<sup>28</sup>

#### 4.1.1.2 Ru SACs

Ru-based catalysts exhibit high activities in the traditional Haber-Bosch process and have been considered as a new generation NERR catalyst with a calculated  $\text{N}_2$  reduction overpotential lower than that of Fe.<sup>9</sup> Ru-based SACs have been extensively investigated for NERR from both theory and experiment. By using DFT computations, Liu and coworkers reported that single Ru atoms doped on electron-deficient B (Ru SA/B) exhibited outstanding NERR performance because of high  $\text{N}_2$  affinity, the low energy barrier for formation of  $^*\text{N}_2\text{H}$  and destabilization of  $^*\text{NH}_2$  and  $\text{NH}_3$  species. NERR took place on Ru SA/B *via* the distal pathway with an activation barrier of 0.42 eV, which was much lower than that of flat Ru catalysts (1.08 eV).<sup>30</sup> Recently, the electrocatalytic NERR performance of Ru SACs has been investigated experimentally. Geng and coworkers developed N-doped carbon-supported single Ru atoms (Ru SA/NC) catalyst by pyrolyzing the Ru-containing ZIF (**Fig. 4A**). HRTEM image (**Fig. 4B**) and Extended X-Ray Absorption Fine Structure (EXAFS) spectrum confirm the atomic dispersion of Ru atoms stabilized by the surrounding N atoms serve as active centers for NERR. As a contrast, Ru NP supported on NC (Ru NP/NC) was also synthesized by increasing the ratio of Ru/Zn in the precursors. The resultant Ru SA/NC catalyst exhibited an FE of 29.6% for NERR at -0.2 V (vs. RHE) in 0.05 M  $\text{H}_2\text{SO}_4$ , twice that of Ru NP/NC (**Fig. 4D and E**), and an  $\text{NH}_3$  yield rate of 120.9  $\mu\text{g/h/mg}_{\text{cat}}$ , which was an order of magnitude higher than the highest value ever reported. It also showed excellent durability with less than 7% decay of the  $\text{NH}_3$  yield rate after 12 h test. Moreover, the Ru SA/NC displayed approximated FE of  $\text{NH}_3$  production in different electrolytes of various pH values, suggesting versatile applications of the catalyst. DFT calculation and temperature-programmed  $\text{N}_2$  desorption results revealed that the excellent NERR performance of Ru SA/NC was attributed to the strong binding strength of  $\text{N}_2$  on single Ru atoms. In addition, the Gibbs free energy change ( $\Delta G$ ) of  $^*\text{N}_2$  dissociation, the rate-limiting step, was much lower on Ru SA/NC than that on Ru NP/NC (**Fig. 4C**), leading to an enhanced NERR performance.<sup>31</sup>

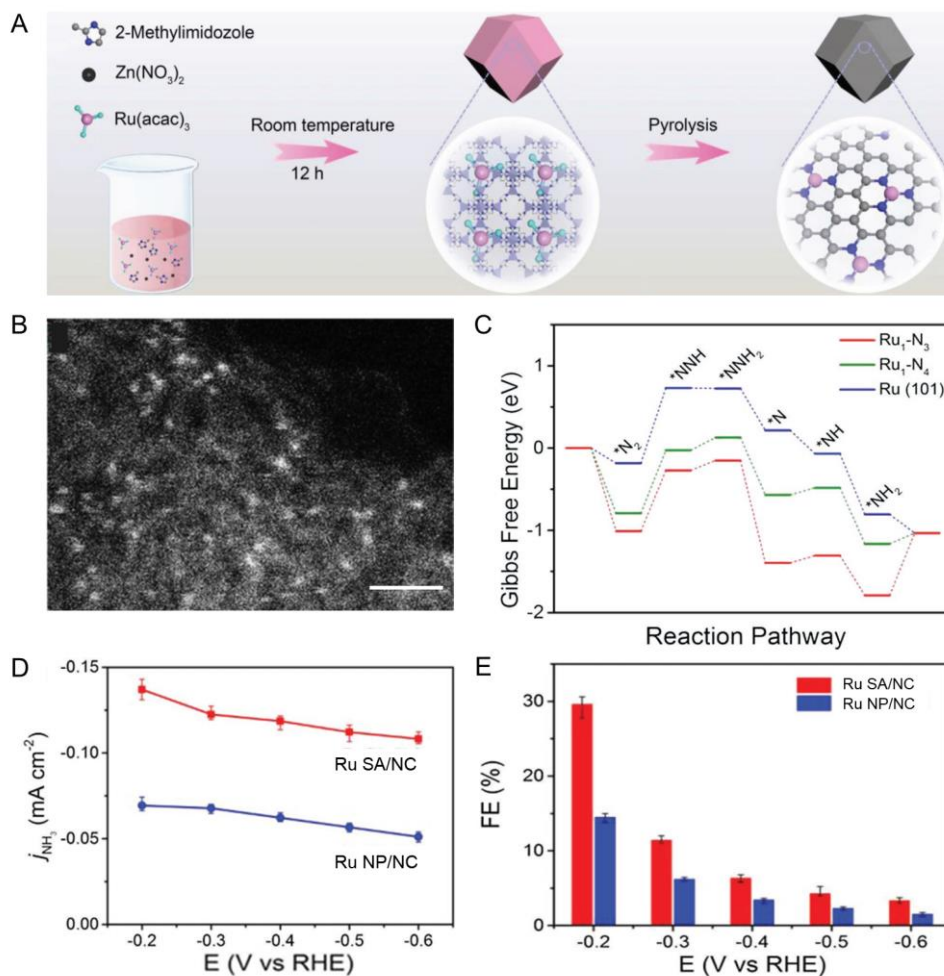


**Fig. 4** Preparation, characterization, calculation and performance of Ru SACs. (A) Schematic representation of the synthetic strategy for Ru SA/NPC. (B) HAADF-STEM image of Ru SAs/N-C (Scale bar: 1 nm). (C) Calculated free energy profile for NERR on various catalysts including  $\text{Ru}_1\text{-N}_3$ ,  $\text{Ru}_1\text{-N}_4$ , and  $\text{Ru (101)}$  with a distal pathway. Current densities (D) and FE (E) of  $\text{NH}_3$  production at different potentials on Ru SA/NPC and Ru NPs/NPC. Reproduced with permission from ref. <sup>31</sup>. Copyright 2018, Wiley-VCH.

It has been well-known that at an increased negative potential, the catalyst surface (especially for metal catalyst) would be thermodynamically covered by H adsorption ( $\text{*H}$ ) than  $\text{N}_2$ , which not only facilitates undesirable HER process, but also blocks the active sites for NERR, resulting in a significantly decreased FE. Therefore, suppressing the H adsorption on the catalyst has been considered an efficient approach to improve FE and selectivity of the catalysts for NERR. Most recently, Tao and coworkers reported that the synergistic effect between single atoms and supports could promote their NERR performance.<sup>9</sup> NPC supported single Ru atom ( $\text{Ru SA/NPC}$ ) synthesized through a coordination-assisted strategy exhibited high activity for  $\text{N}_2$  electroreduction with an  $\text{NH}_3$  yield rate of  $3.665 \text{ mg/mg}_{\text{Ru}}/\text{h}$  at  $-0.21 \text{ V}$ , two times higher than that of the best catalysts ever reported. Interestingly, the addition of  $\text{ZrO}_2$  was found to significantly promote the NERR by suppressing the competitive HER. After the addition of

ZrO<sub>2</sub>, the single Ru atoms were observed to be embedded at ZrO<sub>2</sub> and NPC (Ru@ZrO<sub>2</sub>/NPC), since the O vacancies in ZrO<sub>2</sub> can bind Ru atoms and improve their stability. DFT calculation reveals that NERR mainly occurred at Ru atoms anchored at the O vacancies, which could stabilize the intermediate product, \*NNH (\*N<sub>2</sub> + (H<sup>+</sup> + e<sup>-</sup>) → \*NNH)), by reducing their formation free energy. Therefore, the initiation of the NERR process could be promoted because the formation of \*NNH has been considered as the rate-limiting step in NERR on most metal catalysts. ZrO<sub>2</sub> with O vacancy (Zr<sub>32</sub>O<sub>63</sub>) itself was inactive for NERR, however, Zr<sub>32</sub>O<sub>63</sub> could significantly inhibit the competitive HER on Ru@Zr<sub>32</sub>O<sub>63</sub>, evidenced by much-reduced H adsorption free energy for Ru@Zr<sub>32</sub>O<sub>63</sub>. As a result, Ru@ZrO<sub>2</sub>/NPC delivered a stable NERR behavior over 60 h and 21% of faradic efficiency at -0.11 V. The outstanding NERR performance of Ru SACs was attributed to the atomic dispersion of Ru, HER-suppression effect of ZrO<sub>2</sub>, enhanced N<sub>2</sub> adsorption and low energy barrier for the first protonation of N<sub>2</sub>.<sup>9</sup> In addition, other precious metal (such as Rh and Os)-based SACs have been predicted as potential catalysts for NERR.<sup>32</sup> However, most of them have not yet been experimentally examined.

#### 4.1.2 Non-precious metal-based SACs

Despite their excellent NERR performance, wide application of the precious metal-based catalysts has been restricted because of low abundance, high cost, and short catalyst life. Non-precious metal-based nanostructures have been considered as a candidate of the NERR catalyst. Inspired by the fact that Fe- and Mo-based structures work as the active sites in enzyme nitrogenase, single Fe and Mo atom catalysts are demonstrated to be the most promising candidates for NERR from both experiment<sup>7, 33</sup> and DFT calculation.<sup>34</sup>

#### 4.1.2.1 Fe SACs

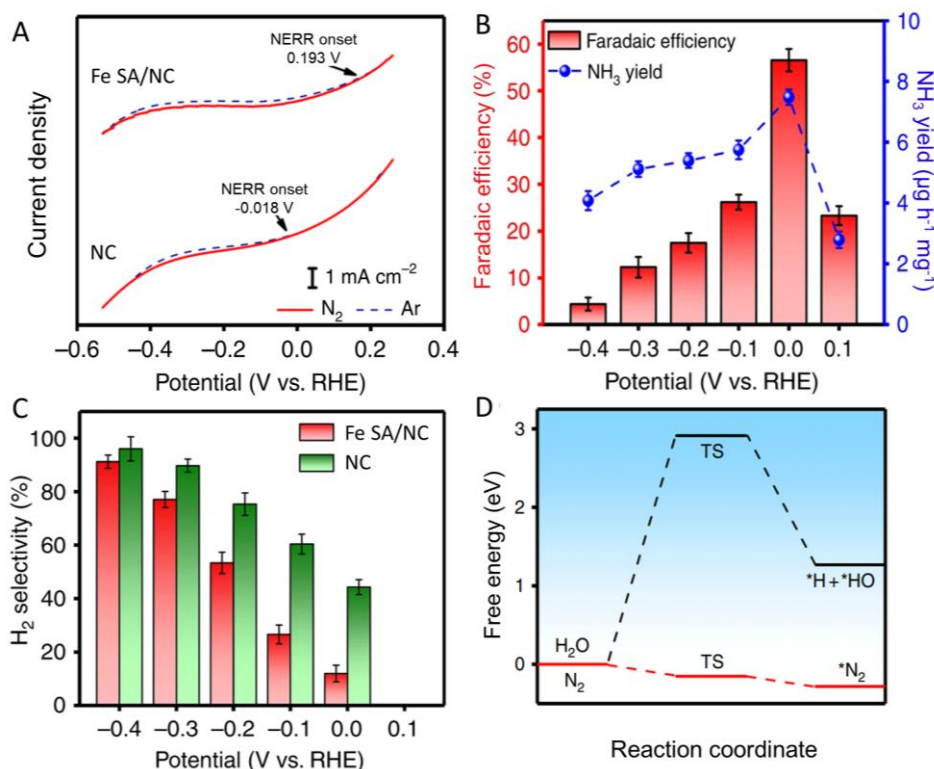


**Fig. 5** The NERR performance of Fe SA/NC and NC. (A) Linear sweep voltammetry (LSV) curves of Fe SA/NC and NC in 0.1 M KOH aqueous solution saturated with Ar and N<sub>2</sub> with a scan rate of 50 mV/s. (B) NH<sub>3</sub> FEs and yield rates of Fe SA/NC at different potentials. (C) H<sub>2</sub> selectivity profile of Fe SA/NC and NC at each given potential. (D) Calculated free energies of the adsorption between \*H and \*N<sub>2</sub> on Fe SA/NC. Reproduced with permission from ref. <sup>8</sup>. Copyright 2019 Nature Publishing Group.

Fe has been recognized as the active center in both Haber-Bosch process and biological nitrogen fixation. With this in mind, Fe SACs are expected as efficient catalysts for NERR. The NERR is typically hindered by a high reaction barrier and competing HER, which leads to a low FE. Synthesizing the catalysts with a positive N<sub>2</sub> reduction potential is an efficient way to suppress the HER because the theoretical potential of HER is 0 V. To this aim, Wang and coworkers synthesized single Fe atoms supported on NC (Fe SA/NC), which exhibited a positive-shifted onset potential of NERR at 0.193 V (**Fig. 5A**), which is much higher than that of NC (-0.018 V). Therefore, the Fe SA/NC afforded a superior FE of 56.55% and a high NH<sub>3</sub> yield rate of 7.48 μg/h/mg at 0 V (**Fig. 5B**), because the HER is greatly suppressed under this potential. Compared with the NC substrate, Fe SA/NC are superior in terms of FE, yield rate and selectivity over the whole tested potentials (**Fig. 5C**). The decreased valence state of Fe in the initial NERR process facilitates the N<sub>2</sub> binding to Fe sites by donating electrons from N<sub>2</sub> to unoccupied *d* orbitals of Fe. DFT simulation results revealed that both \*H (dissociated from water) adsorption and subsequent desorption to form H<sub>2</sub> requires high energy, indicating a significantly suppressed HER. On the other hand, N<sub>2</sub> adsorption on Fe sites was calculated to

be an exothermic process (**Fig. 5D**), which favors the subsequent hydrogenation process and leads to the excellent NERR performance with high NERR selectivity.<sup>8</sup>

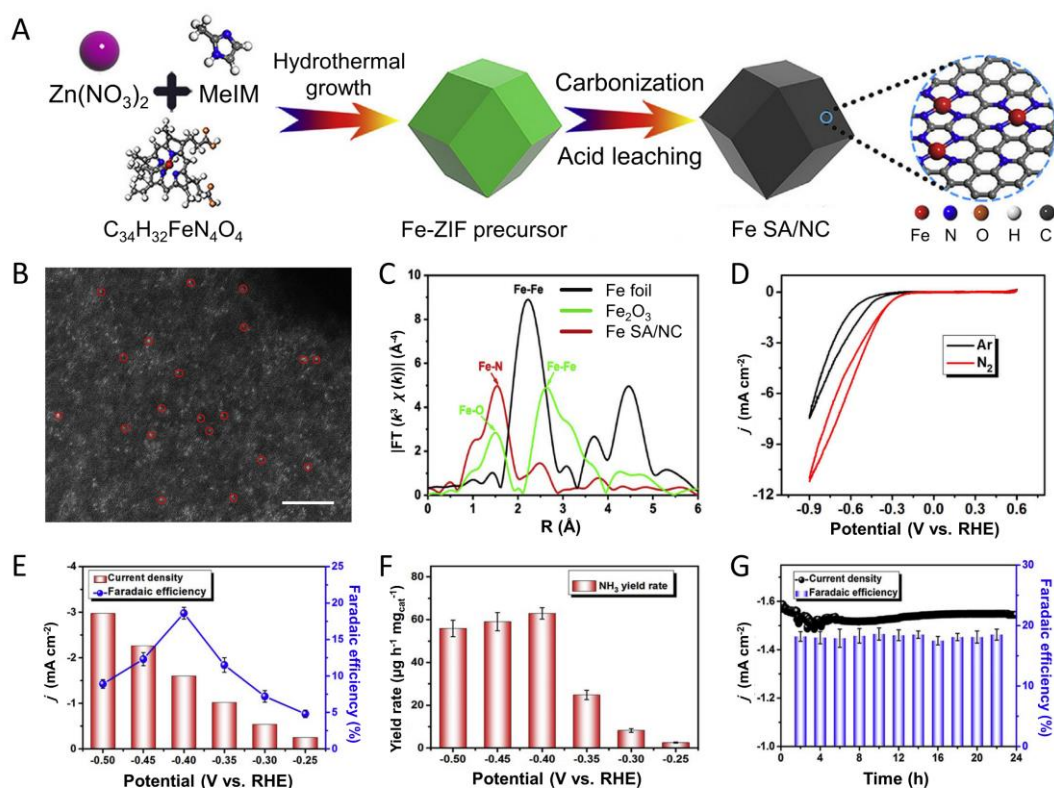


**Fig. 6** The preparation, characterization and NERR performance of Fe SACs. (A) Schematic synthesis of Fe SA/NC. (B) HAADF-STEM image of Fe/SA/NC, scale bar: 2 nm. (C) EXAFS profile of Fe SA/NC. (D) CV curves of Fe SA/NC in N<sub>2</sub>- and Ar-saturated 0.1 M PBS solutions. (E) Electrocatalytic current densities and FE values of Fe SA/NC in 0.1 M PBS solution saturated with N<sub>2</sub> at given potentials. (F) NH<sub>3</sub> yield rate at different potentials. (G) NERR stability test of Fe SA/NC over 24 h. Reproduced with permission from ref. <sup>33</sup>. Copyright 2019, Elsevier Ltd.

Most reported SACs for NERR are working in acidic or alkaline electrolytes, and these corrosive electrolytes easily cause the erosion of the substrate and destabilization of the single atoms. The neutral aqueous electrolyte is considered environment-friendly because it can reduce the corrosion issue and cut down the cost of the electrochemical system. For the first time, Liu and coworkers have developed neutral aqueous electrolyte-working Fe-based SACs for efficient NERR through hydrothermal and anneal treatments of the mixture of Fe/Zn-containing ZIF (**Fig. 6A**). Fe atoms are atomically dispersed on the NC (**Fig. 6B**). From the extended X-ray absorption fine structure (EXAFS) fitting analysis, it can be found that the active center, atomically dispersed Fe atom, is coordinated by four surrounding N atoms (**Fig. 6A**), and the corresponding Fe-N bond distance was measured as 1.5 Å (**Fig. 6C**). The as-prepared Fe SA/NC exhibits a high selectivity toward NERR (**Fig. 6D**), an FE of 18.6% (**Fig. 6E**) and an NH<sub>3</sub> yield rate of 62.9 μg/h/mg<sub>cat</sub> (**Fig. 6F**), as well as high durability (slight decay over 24 h test) at -0.4 V in 0.1 M phosphate buffer solution (PBS, **Fig. 6G**). The excellent

performance for NERR is ascribed to the high density of atomically dispersed Fe-N<sub>4</sub> species in the catalysts. DFT calculation reveals that the Fe atoms coordinated with N can donate the electrons to adsorbed N<sub>2</sub> to elongate the N≡N bond length, and thus facilitate the subsequent hydrogenation of the adsorbed N<sub>2</sub>.<sup>33</sup>

#### 4.1.2.2 Mo SACs

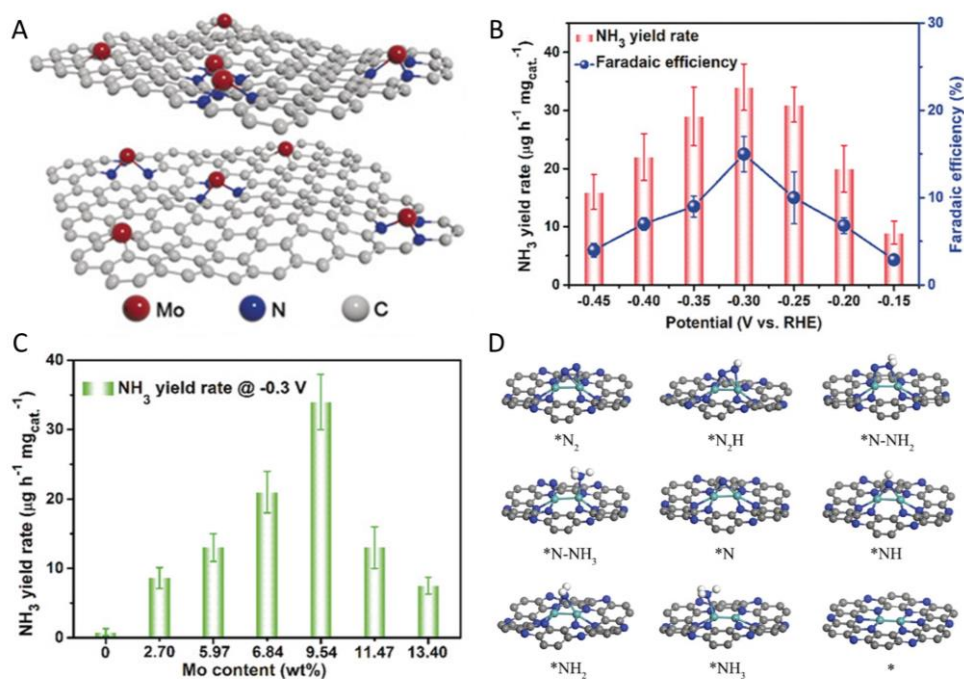


**Fig. 7** Proposed structures and catalytic activities of Mo SACs. (A) Atomic structure model of Mo-SA/NPC. (B) FE (blue) and NH<sub>3</sub> yield rate (red) at different potentials. (C) NH<sub>3</sub> yield rates of Mo-SA/NPC catalysts with different Mo loading amounts. Reproduced with permission from ref. <sup>7</sup>. Copyright 2019 Wiley-VCH. (D) Proposed configurations of the intermediate of each step on the active centers of Mo<sub>2</sub>/C<sub>2</sub>N. Reproduced with permission from ref. <sup>35</sup>. Copyright 2018 Royal Society of Chemistry.

Considering the active centers of most nature nitrogenases are Mo-based structures, Mo SACs would be an efficient NERR catalyst. Han and coworkers synthesized single Mo atoms anchored on NPC through pyrolysis of the mixture of glucose, (NH<sub>4</sub>)<sub>6</sub>Mo<sub>7</sub>O<sub>24</sub> and NH<sub>2</sub>OH·HCl.<sup>7</sup> The single Mo atoms are stabilized *via* the formation of C-Mo and N-Mo bonds (**Fig. 7A**), confirmed by XPS and XANES results. **Fig. 7B** indicates that the as-prepared Mo SA/NPC catalyst with a high Mo loading of 9.54 wt% exhibits high NH<sub>3</sub> yield rate of 34.0  $\mu\text{g}/\text{mg}_{\text{cat}}/\text{h}$  (31.5  $\mu\text{g}/\text{mg}_{\text{cat}}/\text{h}$ ) and FE of 14.6% (6.8%) at -0.3 V (-0.25 V) in 0.1 M KOH (0.1 M HCl) which is attributed to the porous carbon structure and a large number of active sites (Mo-N) because Mo-N was reported to active \*N<sub>2</sub>, stabilize \*N<sub>2</sub>H and destabilize \*NH<sub>2</sub> species.<sup>34</sup> However, Mo nanoclusters appeared after further increment of the Mo content, and the electrocatalytic performance declined by reducing the amount of Mo-N sites (**Fig. 7C**), which confirmed the critical role of single Mo atoms in NERR.<sup>7</sup> With an aid of first-principles



computations, dual Mo atoms anchored C<sub>2</sub>N (Mo<sub>2</sub>/C<sub>2</sub>N) was predicted to show the best NERR performance among many other TM-based catalysts.<sup>35</sup> As shown in **Fig. 7D**, N<sub>2</sub> was firstly adsorbed on the Mo<sub>2</sub>N<sub>6</sub> with a side-on configuration, and the N–N bond was elongated to 1.21 Å by the interaction between \*N<sub>2</sub> and catalyst. Then the \*N<sub>2</sub> would be hydrogenated by an adsorbed proton with a barrier of 0.31 eV, which led to an increased N–N bond of 1.33 Å. In turn, \*NNH was hydrogenated much easier (0.25 eV) because of the decreased bond energy. Finally, N<sub>2</sub> was reduced in a distal way to release the first NH<sub>3</sub>. The remaining N will be successively hydrogenated to produce the second N<sub>2</sub>. The enhanced NERR performance was ascribed to the following factors: 1) N atoms with negative charge could fix Mo atoms firmly; 2) Mo<sub>2</sub>N<sub>6</sub> moieties act as the active center to donate electrons to the antibonding orbital of N<sub>2</sub> to facilitate the activation of N<sub>2</sub>; 3) the weak HER activity on Mo<sub>2</sub>/C<sub>2</sub>N.<sup>35</sup>

#### 4.1.2.3 Others

Besides Fe and Mo, other metal-based SACs have been predicted as potential catalysts for NERR through computing studies. For example, single W atoms coordinated with three C atom embedded in graphene (WC<sub>3</sub>) were selected as a promising catalyst through a high-throughput screening analysis among hundreds of TM-based SAC candidates.<sup>25</sup> Ni SA/WS<sub>2</sub> shows energy-efficient and good stability for NERR because it could accept electrons from \*N<sub>2</sub> to waken the bonding energy of N≡N. Zhao and coworkers identified that the single Mo/Cr atoms on NG (Mo SA/NG and Cr SA/NG) as candidate NERR catalysts based on the calculations in terms of stability, competitive adsorption of N<sub>2</sub> and H, and formation potential of \*NNH and \*H on metal sites.<sup>36</sup> Co dimer anchored on graphdiyne (Co<sub>2</sub>/graphdiyne) was evaluated as a good NERR catalyst among TM (Co, Ni, Fe, and Mn) monomer, dimer and trimer stabilized on graphdiyne monolayers because of the HER-suppressing effect of Co<sub>2</sub>/graphdiyne and strong electron-donating ability of graphdiyne monolayer.<sup>37</sup> These investigations not only present a series of promising NERR catalysts, but also provide important guidance for the rational design of excellent catalysts for NERR.

## 4.2 Metal-free SACs

TM-based SACs deliver excellent NERR performances, however, there are still some intrinsic drawbacks: the d electrons of TMs facilitate the adsorption of H<sup>+</sup> and subsequent HER; TMs in SACs might be released in some harsh conditions.<sup>38</sup> Fortunately, metal-free catalysts exhibit weak H adsorption and better stability. It is worth mentioning that heteroatoms doping could tailor the electronic structure of carbon materials due to the strong electronegativity of heteroatoms and consequent high positive charge density of the adjacent carbon atoms, which has been proved as an efficient way to boost their catalytic performance. With this in mind, the catalytic performance of metal-free SACs for NERR has been explored.

### 4.2.1 B-SACs

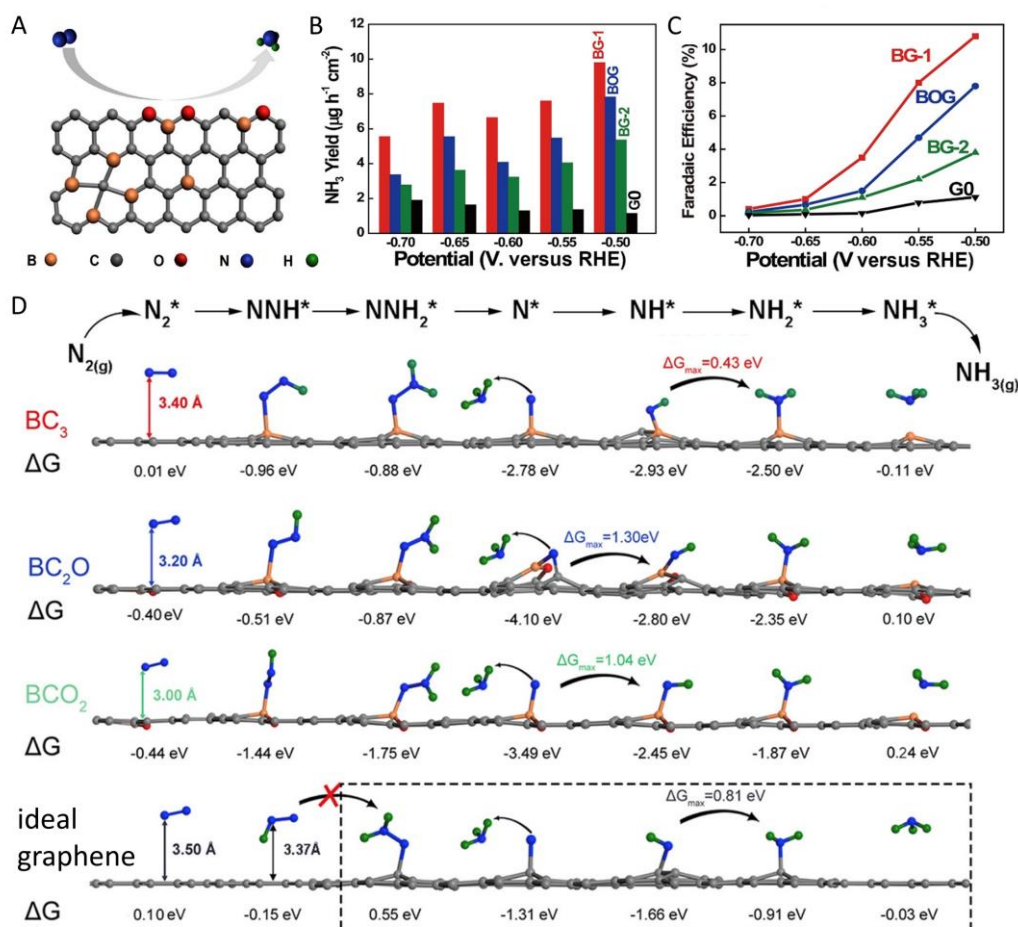


**Fig. 8** Experimental results and theoretical prediction of B doped G for NERR. (A) Proposed B-doped G with different coordination types. The NH<sub>3</sub> production rates (B) and FE (C) of BG-1, BOG (same as BG-1 except thermal treatment under Ar), BG-2, and G at different potentials. (D) Reaction pathways and the corresponding energy changes of NERR on indicated catalysts. Reproduced with permission from ref. <sup>39</sup>. Copyright 2018, Cell Press.

The electron-deficient B could efficiently tune the electronic structure of the carbon nanomaterials. For example, after being doped with B, graphene could remain its original sp<sup>2</sup> hybridization and planar structure. Because of the smaller electronegativity of B than C, B atoms are ready to be positively charged in B doped carbon materials, which would promote NERR by enhancing the capture and stabilization of N<sub>2</sub> by forming B→N π-back bonding and prohibiting H<sup>+</sup> binding. In view of this, Zheng and coworkers developed B-doped graphene (BG) by annealing treatment of lyophilized mixtures of boric acid and graphene oxide (GO) with different mass ratios (5:1, 1:10 and 0:1, and the products are denoted as BG-1, BG-2, and G0) under H<sub>2</sub>/Ar atmosphere. The mixture of boric acid and GO (mass ration of 5:1) treated under Ar atmosphere was denoted as BOG. As expected, BG samples exhibited much-enhanced chemisorption of N<sub>2</sub> than that of G, and higher B doping leads to improved N<sub>2</sub> adsorption. Among these catalysts, BG-1 displayed the best NERR performance in terms of NH<sub>3</sub> yield rate (**Fig. 8B**) and FE of NERR (**Fig. 8C**) under different potentials. The various N doping types



are  $\text{BC}_3$ ,  $\text{BCO}_2$ ,  $\text{BC}_2\text{O}$  (**Fig. 8A**). The distal pathway of NERR is dominant for metal-free catalysts. After evaluation of the  $\text{N}_2$  binding energies, distance and interaction between  $\text{*N}_2$  and various types of B atoms, the balance between  $\text{N}_2$  adsorption and  $\text{NH}_3$  desorption on the catalysts and formation energies of each intermediate,  $\text{BC}_3$  was predicted to possess the lowest energy barrier for NERR (**Fig. 8D**). Based on the experimental measurements and theoretical calculations, the graphene-like BG is a promising metal-free catalyst for NERR.<sup>39</sup>

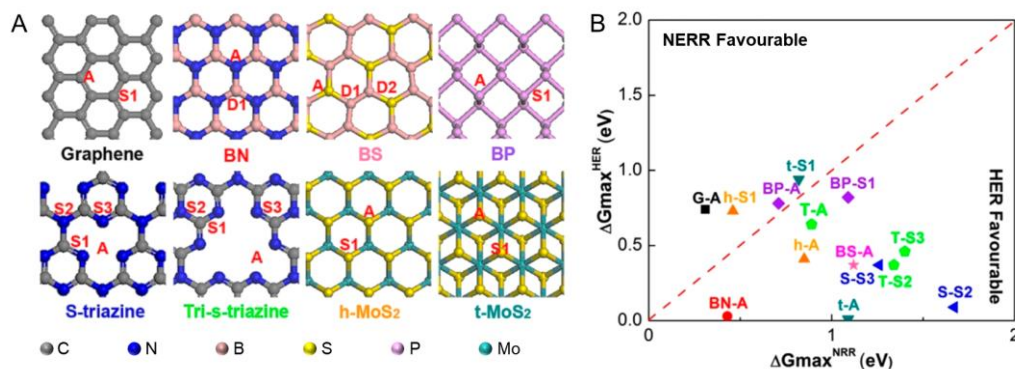


**Fig. 9** Proposed structures and calculation Gibbs free energy of various B SACs. (A) Proposed B SACs models by incorporating B atoms on various 2D materials. (B) Maximum Gibbs free energy of various catalysts for HER and NERR. Reproduced with permission from ref. <sup>40</sup>. Copyright 2019, American Chemical Society.

On the other hand, B atom has three valence electrons, so it with  $\text{sp}^3$  hybridization contains both empty and occupied orbitals. It has been proved that these B atoms can bind  $\text{N}_2$  via a side-on configuration according to the compatibility of the symmetry of the orbitals.<sup>26</sup> Although several B-based catalysts have been developed, the relationship between the states (chemical environment) of B and the NERR performance is poorly known. Sun and coworkers performed a DFT calculation on various B-based SACs for NERR. Unlike metal-based SACs that require empty  $d$  orbitals to accept the lone-pair electrons of  $\text{N}_2$ ,  $\text{B} \rightarrow \text{N} \pi$  back bonding could be formed between  $\text{N}_2$  and B-based SACs, which facilitates the adsorption of  $\text{N}_2$  and weakens the bond energy of  $\text{N}_2$ , and therefore lower the  $\text{N}_2$  activation barriers. Three states of B, including adsorbed, substituted and lattice B atoms on eight common substrates, and a total of 21 catalysts have been studied (**Fig. 9A**). The stability simulation of the catalysts including adsorption, cohesive and formation energies indicate that the proposed single B-based structures are stable and can be synthesized. Consistent with the previous report,<sup>39</sup> this research also reveals that the coexistence of occupied and unoccupied states is necessary for B-based NERR catalysts. In addition, the performance of the catalysts for NERR is highly associated with the charge transfer between B and the substrates. Finally, single B atoms substituted into  $\text{MoS}_2$  and stabilized by graphene are calculated to be the most promising NERR catalysts, presenting superb energy efficiency toward NERR and excellent selectivity against HER (**Fig. 9B**).<sup>40</sup>

## 4.2.2 Others

In addition, NC, O-doped graphene (OG) and S-doped carbon nanosphere (S/CNS) have been developed for NERR. Deriving from zinc-based zeolitic imidazolate frameworks (ZIF-8), metal-free NC was successfully synthesized by Mukherjee and coworkers through a thermal treatment.<sup>41</sup> As expected, the 3D framework construction of the MOF reserved and the defect-rich nanoporous structure was formed by the removal of Zn during the thermal process. The N doping and the graphitization degree could be regulated by changing the annealing conditions to optimize the electronic and geometric structures of NC. The as-synthesized NC exhibited encouraging activity and stability toward NERR, i.e. a high  $\text{NH}_3$  yield rate of  $3.4 \mu\text{mol}/\text{cm}^2/\text{h}$  (7.3 at  $60^\circ\text{C}$ ) and FE of 10.2% at -0.3 V at ambient condition. DFT results revealed that the active centers, that is, the moiety consists of carbon vacancy and three pyridinic N atoms embedded in a carbon plane, shows a strong affinity to  $\text{N}_2$  and favors subsequent  $\text{N}\equiv\text{N}$  cleavage. Surprisingly, additional Fe doping greatly decreases the NERR activity of the NC catalyst, because Fe may block the active center by coordinating with pyridinic N. This work paves a new way for design of efficient NERR catalysts.<sup>41</sup> Similarly, NPC was synthesized from the pyrolysis of ZIF-8 and used as a low cost and metal-free electrocatalyst for NERR. Its high content of pyridinic N and pyrrolic N favors  $\text{N}_2$  adsorption and subsequent  $\text{N}\equiv\text{N}$  cleavage, which leads to enhanced kinetics of  $\text{NH}_3$  synthesis. The alternative mechanism of  $\text{N}_2$  reduction on NPC was revealed by DFT calculations. This finding provides new insight into construct cost-effective and efficient electrocatalysts for NERR.<sup>42</sup> On the one hand, a group of NC catalysts exhibit an improved catalytic activity in NERR because of the N-containing active centers. On the other hand, N-containing catalysts undergo decomposition during the NERR. Smarter design of the stable N-containing catalysts and more rational/comprehensive testing measurements should be conducted to ensure  $\text{NH}_3$  is solely produced from the  $\text{N}_2$  reduction. S/CNS was reported as an efficient catalyst for the reduction of  $\text{N}_2$  to  $\text{NH}_3$  in a neutral electrolyte. S/CNS achieves an  $\text{NH}_3$  yield of  $19.07 \mu\text{g}/\text{mg}_{\text{cat}}/\text{h}$  and an FE of 7.47% at -0.7 V, which are much higher than those of undoped CNS ( $3.7 \mu\text{g}/\text{mg}_{\text{cat}}/\text{h}$  and 1.45%). The as-synthesized S/CNS exhibited high structural stability and great electrocatalytic durability for NERR.<sup>43</sup> In addition, the NERR performance of OG has been investigated. DFT results reveal that compared with the C–O group, both the O–C=O and C=O groups contribute more significant role to the NERR.<sup>44</sup>

**Table 1.** Summary of catalytic performances for both SACs and related nanocatalysts on NERR.

Catalysts	SA content (wt.%)	Catalyst loading (mg/cm <sup>2</sup> )	Electrolyte	E (V) <sup>a</sup>	FE (%)	Yield rate of $\text{NH}_3$	ref
Au SA/C <sub>3</sub> N <sub>4</sub>	0.15	0.48	5 mM H <sub>2</sub> SO <sub>4</sub>	-0.1	11.1	1.305 mg/mg <sub>Au</sub> /h	<sup>28b</sup>
Au SA/NPC	0.205	0.6	0.1 M HCl	-0.2	12.3	2.32 $\mu\text{g}/\text{cm}^2/\text{h}$	<sup>6</sup>
Au cluster (0.5 nm) on TiO <sub>2</sub>	1.542	–	0.1 M HCl	-0.2	8.11	21.4 $\mu\text{g}/\text{mg}_{\text{cat}}/\text{h}$	<sup>10</sup>
Ru SA/NC	0.18	0.255	50 mM H <sub>2</sub> SO <sub>4</sub>	-0.2	29.6	120.9 $\mu\text{g}/\text{mg}_{\text{cat}}/\text{h}$	<sup>31</sup>

						30.84 $\mu\text{g}/\text{cm}^2/\text{h}$	
Ru SA/NPC	0.1	–	0.1 M HCl	-0.21	15; 21 <sup>c</sup>	3.665 $\text{mg}/\text{mg}_{\text{Ru}}/\text{h}$	9
Ru NPs	–	1.7	0.01 M HCl	0.01 -0.1	5.4 –	– 0.55 $\mu\text{g}/\text{cm}^2/\text{h}$	45
Mo SA/NPC	9.54	1	0.1 M KOH 0.1 M HCl	-0.3 -0.25	14.6 $\pm$ 1.6 6.7 $\pm$ 0.3	34.0 $\pm$ 3.6 $\text{mg}/\text{mg}_{\text{cat}}/\text{h}$ 31.5 $\pm$ 1.2 $\text{mg}/\text{mg}_{\text{cat}}/\text{h}$	7
Fe SA/NC	4.2	1	0.1 M PBS	-0.4	18.6 $\pm$ 0.8	62.9 $\pm$ 2.7 $\mu\text{g}/\text{mg}_{\text{cat}}/\text{h}$	33
Fe SA/NC	1.09	1	0.1 M KOH	0	56.55	7.48 $\mu\text{g}/\text{mg}_{\text{cat}}/\text{h}$	8
Fe doped TiO <sub>2</sub>	2.8 <sup>d</sup>	0.1	0.5 M LiClO <sub>4</sub>	-0.4	25.6	25.47 $\mu\text{g}/\text{mg}_{\text{cat}}/\text{h}$	46
Fe/Fe <sub>3</sub> O <sub>4</sub>	–	0.3	0.1 M PBS	-0.3	8.29	0.19 $\mu\text{g}/\text{cm}^2/\text{h}$	47
B SA/G	6.2	0.178	50 mM H <sub>2</sub> SO <sub>4</sub>	-0.5	10.8	9.8 $\mu\text{g}/\text{cm}^2/\text{h}$	39
S-doped CNS	1.21	0.1	0.1 M Na <sub>2</sub> SO <sub>4</sub>	-0.7	7.47	19.07 $\mu\text{g}/\text{mg}_{\text{cat}}/\text{h}$	43
CNS	–				1.45	3.7 $\mu\text{g}/\text{mg}_{\text{cat}}/\text{h}$	
O-doped G	–	–	0.1 M HCl	-0.55 -0.45	– 12.6	21.3 $\mu\text{g}/\text{mg}_{\text{cat}}/\text{h}$ –	44
NC	–	0.8	0.1 M KOH	-0.3	10.2	3.4 $\mu\text{mol}/\text{cm}^2/\text{h}$	41
NPC	13.6 (at%)	0.6	50 mM H <sub>2</sub> SO <sub>4</sub>	-0.9	1.42	1.40 $\text{mmol}/\text{g}_{\text{cat}}/\text{h}$	42

CNT = carbon nanotube. <sup>a</sup>vs. RHE; <sup>b</sup>synthesized from N<sub>2</sub> and H<sub>2</sub>; <sup>c</sup>measured at 0.17 V, <sup>d</sup>the mass ratio of Fe over Ti.

Most reported SACs and related nanocatalysts for NERR have been summarized in **Table 1**. It can be found that SACs exhibit much higher FE than that of corresponding traditional nanocatalysts, which is ascribed to the unique topographic and electronic structures of the SACs and their consequent effects on suppressing HER. Taking the loading amount of catalysts and the content of active atoms (mainly for metal atoms) into account, the greatly enhanced NH<sub>3</sub> yield rate was obtained on SACs due to the highly exposed single atoms and improved intrinsic activities derived from the unsaturated coordination and enhanced interactions between single atoms and substrates. Currently, Ru and Fe SACs are superior to others in terms of both FE and yield rate of NH<sub>3</sub>. It should be noted that nonmetal-based SACs present substantial NERR performance because nonmetallic atoms could tailor the electronic structure of carbon substrates.

## 5. Summary and perspectives

NERR has been regarded as a promising alternative to the traditional Haber-Bosch process. An increasing number of works aiming at synthesizing novel electrocatalysts with excellent NERR performance have been published and some encouraging results have been obtained. However, most of the catalysts are suffering from the poor FE, low NH<sub>3</sub> yield rate and poor selectivity against HER due to the low affinity of N<sub>2</sub> on the catalysts, high overpotential and high energy barrier raised from intrinsic nature of the catalysts. Fortunately, SACs have emerged as promising NERR electrocatalysts because of the unique structural and electronic characteristics and high atom efficiency. Enormous progress for NERR has been achieved through rational

design and ingenious synthesis of novel SACs including precious metal-, nonprecious metal- and nonmetal-based SACs. Nevertheless, considerable scientific and technical challenges still exist to promote the wide commercialization of NERR. First of all, the performance of the current SACs for NERR is limited in terms of low activity and selectivity. For example, some catalysts exhibit excellent NERR performance at a relatively high potential. However, at an increased negative potential, all of the catalysts experience dramatically decreased FE and  $\text{NH}_3$  yield rate because of the thermodynamically favored H than  $\text{N}_2$  adsorption on catalysts, resulting in the limitation of  $\text{N}_2$  transport and predominance of HER.<sup>6</sup> Moreover, the mechanism of NERR remains an open debate because of the structural complexity and diversity of the typical catalysts, which therefore constitute obstacles for reasonable design and development of advanced NERR catalysts.<sup>12</sup> Therefore, it is urgent and challenging to synthesize novel SACs with efficient and stable NERR activity.

The following strategies should be considered for the design and fabrication of the adequate NERR SACs and the development of NERR. (1) NERR involves multiple electron and proton transfer steps and is a complicated process. It is essential to fully understand the structure-performance relationship and catalytic mechanism of NERR at the atomic level for the rational design of the catalysts.<sup>17</sup> More SACs of various single atoms and supports couples should be proposed to expand the library of catalysts for the search of outstanding candidate SACs, which in turn contribute to reveal the mechanism and guide the design of the SACs. (2) The local environment of the SACs could be regulated to suppress the competing HER. For example, hydrophobic polymers with porous structures were incorporated into the catalyst to obstruct  $\text{H}_2\text{O}$  adsorption on the catalyst surface and thus improve a higher  $\text{NH}_3$  yield rate and FE.<sup>48</sup> It is preferred to build an aerophilic-hydrophilic interface between the electrolyte solution and catalysts to simultaneously facilitate the diffusion of  $\text{N}_2$  and active proton and impede water absorption on the surface of the catalyst surface.<sup>48</sup> (3) Rigorous protocols for precise measurements of  $\text{NH}_3$  exclusively from electroreduction of  $\text{N}_2$  are highly desired. The false positives of  $\text{NH}_3$  from contaminants or catalyst decomposition would lead to serious questions on the accuracy and reliability of the reported results and inaccurate evaluation of the catalysts because of the low activity and selectivity. (4) More ingenious synthetic methods of the catalysts with desired structures should be explored. A large number of SACs have been predicted as excellent catalysts for NERR, however, few of them have been synthesized experimentally because of the difference in microstructures between ideal models and real samples. (5) Catalysts with neighboring single atoms (both homogeneous and heterogeneous) should be explored to make full use of the synergetic interactions between neighboring coupled single atoms to boost the NERR.<sup>49</sup> (6) The effect of cocatalysts should not be ignored. For example, potassium cations ( $\text{K}^+$ ) were found to improve the NERR and simultaneously suppress the HER activity of Bismuth-based catalyst by stabilizing the key  $\text{N}_2$ -reduction intermediates, regulating  $\text{H}^+$  diffusion and suppressing  $\text{H}^+$  reduction in aqueous solutions, resulting in an enhanced NERR performance (FE of 66%).<sup>50</sup> Likewise, Li-mediated NERR was achieved because at the given potential  $\text{Li}^+$  could be reduced to Li, which spontaneously reacts with  $\text{N}_2$

to form  $\text{Li}_3\text{N}$ , which was then protonated to form  $\text{NH}_3$  when using ethanol as a proton carrier. (7) Last but not least, exploring novel electrolyte systems with increased  $\text{N}_2$  solubility is highly desired because the FE of NERR is greatly limited by the low solubility of  $\text{N}_2$  in aqueous solutions especially at higher current densities.<sup>51</sup> These abovementioned issues should be taken into accounts to fully understand the  $\text{N}_2$  reduction process, improve the NERR performance of SACs and develop energy-efficient  $\text{NH}_3$  electrochemical synthesis strategies.

## Acknowledgments

This work was financially supported by the Natural Scientific Foundation of China (21804074), the Natural Scientific Foundation of Shandong Province (ZR2018BB051) and the Open Funds of the State Key Laboratory of Electroanalytical Chemistry (SKLEAC201906)

## Competing financial interests

The authors declare no competing financial interests.

## References

1. G. Soloveichik, *Nat. Catal.*, 2019, **2**, 377-380.
2. Q. Wang, Y. Lei, D. Wang and Y. Li, *Energ. Environ. Sci.*, 2019, **12**, 1730-1750.
3. Y. Fang, Z. Liu, J. Han, Z. Jin, Y. Han, F. Wang, Y. Niu, Y. Wu and Y. Xu, *Adv. Energy Mater.*, 2019, **9**, 1803406.
4. L. Wang, M. Xia, H. Wang, K. Huang, C. Qian, C. T. Maravelias and G. A. Ozin, *Joule*, 2018, **2**, 1055-1074.
5. Z. Liu, Y. Zhong, I. Shafei, R. Borman, S. Jeong, J. Chen, Y. Losovyj, X. Gao, N. Li, Y. Du, E. Sarnello, T. Li, D. Su, W. Ma and X. Ye, *Nature Communications*, 2019, **10**, 1394.
6. Q. Qin, T. Heil, M. Antonietti and M. Oschatz, *Small Methods*, 2018, **2**, 1800202.
7. L. Han, X. Liu, J. Chen, R. Lin, H. Liu, F. Lü, S. Bak, Z. Liang, S. Zhao, E. Stavitski, J. Luo, R. R. Adzic and H. L. Xin, *Angew. Chem. Int. Ed.*, 2019, **58**, 2321-2325.
8. M. Wang, S. Liu, T. Qian, J. Liu, J. Zhou, H. Ji, J. Xiong, J. Zhong and C. Yan, *Nat. Commun.*, 2019, **10**, 341.
9. H. Tao, C. Choi, L.-X. Ding, Z. Jiang, Z. Han, M. Jia, Q. Fan, Y. Gao, H. Wang, A. W. Robertson, S. Hong, Y. Jung, S. Liu and Z. Sun, *Chem*, 2019, **5**, 204-214.
10. M.-M. Shi, D. Bao, B.-R. Wulan, Y.-H. Li, Y.-F. Zhang, J.-M. Yan and Q. Jiang, *Adv. Mater.*, 2017, **29**, 1606550.
11. S. Wang, F. Ichihara, H. Pang, H. Chen and J. Ye, *Adv. Funct. Mater.*, 2018, **28**, 1803309.
12. X. Liu, Y. Jiao, Y. Zheng, M. Jaroniec and S.-Z. Qiao, *J. Am. Chem. Soc.*, 2019, **141**, 9664-9672.
13. Y. Peng, B. Lu and S. Chen, *Adv. Mater.*, 2018, **30**, 1801995.
14. C. Zhu, S. Fu, Q. Shi, D. Du and Y. Lin, *Angew. Chem. Int. Ed.*, 2017, **56**, 13944-13960.
15. Y. Qiu, X. Peng, F. Lü, Y. Mi, L. Zhuo, J. Ren, X. Liu and J. Luo, *Chem. -Asian. J.*, 2019, **14**, 2770-2779.

16. B. Qiao, A. Wang, X. Yang, L. F. Allard, Z. Jiang, Y. Cui, J. Liu, J. Li and T. Zhang, *Nat. Chem.*, 2011, **3**, 634.
17. Y. Chen, S. Ji, C. Chen, Q. Peng, D. Wang and Y. Li, *Joule*, 2018, **2**, 1242-1264.
18. L. Jiao, H. Yan, Y. Wu, W. Gu, C. Zhu, D. Du and Y. Lin, *Angew. Chem. Int. Ed.*, 2019, DOI: DOI: 10.1002/anie.201905645.
19. C. Zhu, Q. Shi, B. Z. Xu, S. Fu, G. Wan, C. Yang, S. Yao, J. Song, H. Zhou, D. Du, S. P. Beckman, D. Su and Y. Lin, *Adv. Energy Mater.*, 2018, **8**, 1801956.
20. W. Chen, J. Pei, C.-T. He, J. Wan, H. Ren, Y. Wang, J. Dong, K. Wu, W.-C. Cheong, J. Mao, X. Zheng, W. Yan, Z. Zhuang, C. Chen, Q. Peng, D. Wang and Y. Li, *Adv. Mater.*, 2018, **30**, 1800396.
21. Q. Shi, C. Zhu, D. Du and Y. Lin, *Chem. Soc. Rev.*, 2019, **48**, 3181-3192.
22. X. Zheng, P. De Luna, F. P. García de Arquer, B. Zhang, N. Becknell, M. B. Ross, Y. Li, M. N. Banis, Y. Li, M. Liu, O. Voznyy, C. T. Dinh, T. Zhuang, P. Stadler, Y. Cui, X. Du, P. Yang and E. H. Sargent, *Joule*, 2017, **1**, 794-805.
23. C. Choi, S. Back, N.-Y. Kim, J. Lim, Y.-H. Kim and Y. Jung, *ACS Catal.*, 2018, **8**, 7517-7525.
24. J. Guo, J. Huo, Y. Liu, W. Wu, Y. Wang, M. Wu, H. Liu and G. Wang, *Small Methods*, 2019, **3**, 1900159.
25. C. Ling, Y. Ouyang, Q. Li, X. Bai, X. Mao, A. Du and J. Wang, *Small Methods*, 2018, **2**, 1800376.
26. C. Ling, X. Niu, Q. Li, A. Du and J. Wang, *J. Am. Chem. Soc.*, 2018, **140**, 14161-14168.
27. Y. Yao, S. Zhu, H. Wang, H. Li and M. Shao, *J. Am. Chem. Soc.*, 2018, **140**, 1496-1501.
28. X. Wang, W. Wang, M. Qiao, G. Wu, W. Chen, T. Yuan, Q. Xu, M. Chen, Y. Zhang, X. Wang, J. Wang, J. Ge, X. Hong, Y. Li, Y. Wu and Y. Li, *Sci. Bull.*, 2018, **63**, 1246-1253.
29. K. Zhang, R. Guo, F. Pang, J. He and W. Zhang, *ACS Sustain. Chem. Eng.*, 2019, **7**, 10214-10220.
30. C. Liu, Q. Li, J. Zhang, Y. Jin, D. R. MacFarlane and C. Sun, *J. Mater. Chem. A*, 2019, **7**, 4771-4776.
31. Z. Geng, Y. Liu, X. Kong, P. Li, K. Li, Z. Liu, J. Du, M. Shu, R. Si and J. Zeng, *Adv. Mater.*, 2018, **30**, 1803498.
32. L. Li, X. Wang, H. Guo, G. Yao, H. Yu, Z. Tian, B. Li and L. Chen, *Small Methods*, 2019, **3**, 1900337.
33. F. Lü, S. Zhao, R. Guo, J. He, X. Peng, H. Bao, J. Fu, L. Han, G. Qi, J. Luo, X. Tang and X. Liu, *Nano Energy*, 2019, **61**, 420-427.
34. J. Zhao and Z. Chen, *J. Am. Chem. Soc.*, 2017, **139**, 12480-12487.
35. X. Zhang, A. Chen, Z. Zhang and Z. Zhou, *J. Mater. Chem. A*, 2018, **6**, 18599-18604.
36. W. Zhao, L. Zhang, Q. Luo, Z. Hu, W. Zhang, S. Smith and J. Yang, *ACS Catal.*, 2019, **9**, 3419-3425.
37. D. Ma, Z. Zeng, L. Liu, X. Huang and Y. Jia, *J. Phys. Chem. C*, 2019, **123**, 19066-19076.

38. R. Zhao, H. Xie, L. Chang, X. Zhang, X. Zhu, X. Tong, T. Wang, Y. Luo, P. Wei, Z. Wang and X. Sun, *EnergyChem*, 2019, **1**, 100011.
39. X. Yu, P. Han, Z. Wei, L. Huang, Z. Gu, S. Peng, J. Ma and G. Zheng, *Joule*, 2018, **2**, 1610-1622.
40. C. Liu, Q. Li, C. Wu, J. Zhang, Y. Jin, D. R. MacFarlane and C. Sun, *J. Am. Chem. Soc.*, 2019, **141**, 2884-2888.
41. S. Mukherjee, D. A. Cullen, S. Karakalos, K. Liu, H. Zhang, S. Zhao, H. Xu, K. L. More, G. Wang and G. Wu, *Nano Energy*, 2018, **48**, 217-226.
42. Y. Liu, Y. Su, X. Quan, X. Fan, S. Chen, H. Yu, H. Zhao, Y. Zhang and J. Zhao, *ACS Catal.*, 2018, **8**, 1186-1191.
43. L. Xia, X. Wu, Y. Wang, Z. Niu, Q. Liu, T. Li, X. Shi, A. M. Asiri and X. Sun, *Small Methods*, 2019, **3**, 1800251.
44. T. Wang, L. Xia, J.-J. Yang, H. Wang, W.-H. Fang, H. Chen, D. Tang, A. M. Asiri, Y. Luo, G. Cui and X. Sun, *Chem. Commun.*, 2019, **55**, 7502-7505.
45. D. Wang, L. M. Azofra, M. Harb, L. Cavallo, X. Zhang, B. H. R. Suryanto and D. R. MacFarlane, *ChemSusChem*, 2018, **11**, 3416-3422.
46. T. Wu, Z. Xing, S. Mou, C. Li, Y. Qiao, Q. Liu, X. Zhu, Y. Luo, X. Shi, Y. Zhang and X. Sun, *Angew. Chem. Int. Ed.*, 2019, DOI: DOI: 10.1002/anie.201911153.
47. L. Hu, A. Khaniya, J. Wang, G. Chen, W. E. Kaden and X. Feng, *ACS Catal.*, 2018, **8**, 9312-9319.
48. J. Zheng, Y. Lyu, M. Qiao, R. Wang, Y. Zhou, H. Li, C. Chen, Y. Li, H. Zhou, S. P. Jiang and S. Wang, *Chem*, 2019, **5**, 617-633.
49. P. Zhou, X. Hou, Y. Chao, W. Yang, W. Zhang, Z. Mu, J. Lai, F. Lv, K. Yang, Y. Liu, J. Li, J. Ma, J. Luo and S. Guo, *Chem. Sci.*, 2019, **10**, 5898-5905.
50. Y.-C. Hao, Y. Guo, L.-W. Chen, M. Shu, X.-Y. Wang, T.-A. Bu, W.-Y. Gao, N. Zhang, X. Su, X. Feng, J.-W. Zhou, B. Wang, C.-W. Hu, A.-X. Yin, R. Si, Y.-W. Zhang and C.-H. Yan, *Nat. Catal.*, 2019, **2**, 448-456.
51. C. S. M. Kang, X. Zhang and D. R. MacFarlane, *J. Phys. Chem. C*, 2018, **122**, 24550-24558.

## Table of content

